SUPPORTING INFORMATION

Probing the Binding Modes of a Multidomain Protein to Lipid-based Nanoparticles by Relaxation based NMR

Alberto Ceccon[†], Vitali Tugarinov[†*], Andrew J. Boughton[‡], David Fushman[‡] and G. Marius Clore[†*]

[†]Laboratory of Chemical Physics, National Institute of Diabetes and Digestive and Kidney Diseases, National Institutes of Health, Bethesda, Maryland 20892-0520
[‡]Department of Chemistry and Biochemistry, Center for Biomolecular Structure and Organization, University of Maryland, College Park, Maryland 20742-4454

Materials and Methods

Preparation of NMR samples.

Covalently linked di-ubiquitin (Ub_2) was constructed via an isopeptide bond linkage formed between the ε-amino group of a lysine side-chain of one monomeric unit (Ub_1), denoted as the 'proximal' domain in what follows, and the C-terminal carboxyl group of another monomeric unit, denoted as the 'distal' domain. Two types of linkages - through the side-chains of endogenous Lys^{63} (K63) and Lys^{48} (K48) of ubiquitin - were used in this study. The K63- and K48-linked Ub_2 were assembled enzymatically employing chain-terminating mutations as described in detail previously.[S1,2] Specifically, the distal domain carried either K48R (in K48-Ub_2) or K63R (in K63-Ub_2) mutations, while the proximal domain had an additional Asp at the C-terminus. In each of the K63- and K48-linked Ub_2 only a single domain, either distal or proximal, was U-[^{15}N/^{2}H]-labeled, with the other domain at natural isotopic abundance and hence 'NMR-silent' in heteronuclear NMR experiments, resulting in a total of four samples of Ub_2 for relaxation-based NMR studies in the absence and presence of lipid-based nanoparticles: (1) distal-U-[^{15}N/^{2}H]-K63-Ub_2, (2) proximal-U-[^{15}N/^{2}H]-K63-Ub_2, (3) distal-U-[^{15}N/^{2}H]-K48-Ub_2, and (4)

proximal-U-[^{15}N/^{2}H]-K48-Ub_2. U-[^{15}N/^{2}H]-labeled mono-ubiquitin (Ub_1) was expressed and purified as described previously.[S1] All NMR samples were prepared in 10 mM phosphate buffer (K_2HPO_4/KH_2PO_4), pH 6.8, and 7% D_2O/93% H_2O. The final concentration of Ub_1 and Ub_2 following the addition of liposome solutions (see below) was 0.22 mM.

Preparation and characterization of diamagnetic and paramagnetic liposomes.

The sodium salt of 1-palmitoyl-2-oleoyl-*sn*-glycero-3-phospho-(1'-*rac*-glycerol) (POPG), the gadolinium salt of 1,2-distearoyl-*sn*-glycero-3-phosphoethanolamine-N-diethylenetriaminepenta-acetic acid (18:0 PE-DTPA-Gd^{3+}) and cholesterol were purchased from Avanti Polar Lipids (Alabaster, AL).

Unilamellar vesicles were prepared by dissolving an aliquot of POPG and 20 % (mol/mol) cholesterol in a chloroform:methanol (2:1) solution. For preparation of paramagnetic vesicles, 10% (mol/mol) of 18:0 PE-DTPA-Gd^{3+} phospholipid was added to the lipid mixture. The solution was dried by slow evaporation of the organic solvent to a thin film on the walls of a round-bottom flask. Any trace of solvent was removed by keeping the lipid thin film under a stream of nitrogen for 3-4 hours. Re-hydration of the film was carried out by vortex agitation in 10 mM phosphate buffer (K_2HPO_4/KH_2PO_4), pH 6.8 to a final lipid stock concentration of 10 mM. For preparation of small unilamellar vesicles (SUV), rehydrated lipids were sonicated without cooling at 15 Watt for at least two 10-min cycles using a probe tip sonicator (Misonix, NY). Any titanium fragments released by the sonication tip were removed by centrifugation (8000 g x 10 minutes). Homogenous large unilamellar vesicles (LUV) were obtained by repeatedly extruding the lipid suspension through polycarbonate filters (successively 1 μm, 400 nm and 100 nm pore sizes) to obtain uniformly sized unilamellar vesicles of ~100 nm in diameter. Liposome solutions were stored in the dark above the transition temperature (T_m) to prevent lipid oxidation. The size distribution of the vesicles was determined using dynamic light scattering (DLS) performed with a Zetasizer Nano ZS (Malvern Instruments, 4 mW He-Ne laser, λ_0 = 633 nm, θ = 173°). The measurements were repeated 5 times after a 2 min. temperature equilibration (25 °C) on 1 mM (in lipid) samples.

NMR relaxation measurements.

All NMR experiments were recorded at 25 °C using Bruker Avance-III spectrometers, equipped with Bruker TCI triple resonance *z*-axis gradient cryogenic probes operating at ^{1}H Larmor frequencies of 700.24 and 500.68 MHz. All measurements in the presence of diamagnetic and paramagnetic POPG vesicles were carried out using protein:lipid ratios of 1:2 (mol/mol).

^{15}N-R_2 values in the absence and in presence of LUV and SUV liposomes were extracted from a combination of HSQC-based ^{15}N $R_{1\rho}$ and R_1 measurements using procedures described previously.[S3,4] A^{15}N spin-lock field strength of 1.8 kHz was employed for the ^{15}N $R_{1\rho}$ measurements to suppress any potential chemical exchange-induced line broadening. The following spin-lock periods were used in the ^{15}N $R_{1\rho}$ experiments: 5, 10, 20, 40 and 60 ms at 700 MHz, and 5, 20, 40, 60 and 80 ms at 500 MHz. ^{15}N-R_1 measurements were performed using delays of 40, 160, 240, 320 and 400 ms. Each 2D experiment comprised 128*× 512* (500 MHz) or 128*× 850* (700 MHz) complex points in the indirect (^{15}N) and direct (^{1}H) dimensions, respectively, corresponding to respective acquisition times of 100 ms and 73 ms at 500 MHz, and 72 ms and 87 ms at 700 MHz. Experiments were acquired with 16 scans per FID and an inter-scan delay of 2.0 s, resulting in net acquisition times of ~16 hr. per experiment.

^{1}H$_N$-R_2 relaxation experiments were carried out using standard procedures.[S5] Relaxation delays of 4, 8, 16, 24, 32 and 40 ms were used for the diamagnetic samples, while the delays of 2, 4, 8, 12, 16 and 20 ms were used for the paramagnetic samples.

NMR spectra were processed using the nmrPipe/nmrDraw suite of programs,[S6] and the relaxation decays were best fit to a single exponential. Errors in the extracted rates were estimated from Monte Carlo simulations. Lifetime line-broadening (ΔR_2) values were calculated as the difference between ^{15}N or ^{1}H$_N$ R_2 values obtained in the presence and absence of LUV/SUV vesicles. Amide proton (^{1}H$_N$) intermolecular transverse PRE rates (Γ_2^{app}) were obtained from the difference between the R_2 rates obtained in the presence of paramagnetic and diamagnetic LUVs.

Calculation of ^{15}N-ΔR_2 in the presence of LUV and SUV liposomes.

In the absence of chemical shift differences between the free and bound states of the protein, the evolution of magnetization between the free (A) and bound (B) states is given by a simplified form of the Bloch-McConnell equations,[S7,S8]

$$\frac{d}{dt}\begin{bmatrix} I^{A} \\ I^{B} \end{bmatrix} = -\begin{bmatrix} R_2^{A} + k_{on}^{app} & -k_{off} \\ -k_{on}^{app} & R_2^{B} + k_{off} \end{bmatrix}\begin{bmatrix} I^{A} \\ I^{B} \end{bmatrix} \qquad \text{(S1)}$$

where I^A and I^B are the transverse magnetizations of states A and B, respectively; k_{off} and k_{on}^{app} are the dissociation and pseudo-first order apparent association rate constants; and R_2^A and R_2^B are the intrinsic transverse relaxation rates in the free and bound states, respectively (in the absence of exchange). ΔR_2 values can be calculated by propagating Eq S1 and 'reading off' the transverse

magnetization of the (observable) state A at two separated time-points assuming single-exponential decay:

$$\Delta R_2 = ln[I^{\mathrm{A}}(\tau_1) / I^{\mathrm{A}}(\tau_2)] / (\tau_2 - \tau_1) \qquad \text{(S2.1)}$$

where the delays τ_1 and τ_2 were set to 10 and 70 ms (for ^{15}N-ΔR_2 LUV) and 10 and 30 ms (for ^{15}N-ΔR_2 SUV). τ_1 was chosen to remove any small deviations from single-exponential behaviour and τ_2 was chosen to match the order of magnitude of the experimental decay.

Approximate solutions of Eq S1 can be obtained by retaining only the leading term in the characteristic polynomial of the evolution matrix on the right-hand side of Eq S1.[S8] Using this approach, it can be shown that ΔR_2 is to a very good approximation given by,

$$\Delta R_2 = k_{\mathrm{on}}^{\mathrm{app}} \frac{\Delta R}{k_{\mathrm{off}} + \Delta R} \approx k_{\mathrm{on}}^{\mathrm{app}} \frac{R_2^{\mathrm{B}}}{k_{\mathrm{off}} + R_2^{\mathrm{B}}} \qquad \text{(S2.2)}$$

where $\Delta R = R_2^{\mathrm{B}} - R_2^{\mathrm{A}} \approx R_2^{\mathrm{B}}$ as for both LUV and SUV interactions $R_2^{\mathrm{B}} >> R_2^{\mathrm{A}}$. Note that in the limit of fast exchange ($k_{\mathrm{off}} >> R_2^{\mathrm{B}}$) and for highly skewed populations ($k_{\mathrm{off}} >> k_{\mathrm{on}}^{\mathrm{app}}$), $\Delta R_2 \approx p_{\mathrm{B}} R_2^{\mathrm{B}}$, where p_{B} is the population of the bound state B.

Calculation of ^{15}N transverse spin relaxation rates in the bound state

In an isolated ^{15}N-H spin-pair, the ^{15}N-R_2 is accounted for by the sum of two mechanisms, ^{15}N-^{1}H dipolar interaction and ^{15}N chemical shift anisotropy (CSA), and is related to molecular motions of Ub_2 on the surface of liposomes through their dependence on linear combinations of the spectral density function J evaluated at a finite number of frequencies ω:[S9]

$$\begin{aligned} {}^{15}\mathrm{N}\text{-}R_2 = {} & 0.05(\gamma_{\mathrm{H}}\gamma_{\mathrm{N}}\hbar < r_{\mathrm{HN}}^{-3} >)^2 [4J(0) + J(\omega_{\mathrm{H}} - \omega_{\mathrm{N}}) + 3J(\omega_{\mathrm{N}}) + 6J(\omega_{\mathrm{H}}) + 6J(\omega_{\mathrm{H}} + \omega_{\mathrm{N}})] \\ & + (1/45)\omega_{\mathrm{N}}^2 (\sigma_{\parallel} - \sigma_{\perp})^2 (3J(\omega_{\mathrm{N}}) + 4J(0)] \end{aligned} \qquad \text{(S3)}$$

where γ_{H} and γ_{N} are the gyromagnetic ratios of ^{1}H and ^{15}N nuclei, respectively; $\hbar$ is Planck's constant divided by 2π; r_{HN} is the N-H bond length (1.02 Å); and ($\sigma_{\parallel}$ - $\sigma_{\perp}$) is the ^{15}N CSA (-170 ppm), where $\sigma_{\parallel}$ and $\sigma_{\perp}$ are the parallel and perpendicular components of the axially symmetric ^{15}N chemical shift tensor. The form of the spectral density function J adopted in this work is specified in Eq. 2 of the main text.

Construction of the target error function.

The minimization of the following error function F was performed in the combined analysis of LUV and SUV ^{15}N-ΔR_2 data for each distal/proximal K63/K48-linked sample of Ub_2,

$$F = \alpha_1 \sum_i \left(\frac{\Delta R_{2,\mathrm{LUV}}^{\mathrm{obs},i} - \Delta R_{2,\mathrm{LUV}}^{\mathrm{calc},i}}{\sigma_{\Delta R_{2,\mathrm{LUV}}}^{i}} \right)^2 + \alpha_2 \sum_i \left(\frac{\Delta R_{2,\mathrm{SUV}}^{\mathrm{obs},i} - \Delta R_{2,\mathrm{SUV}}^{\mathrm{calc},i}}{\sigma_{\Delta R_{2,\mathrm{SUV}}}^{i}} \right)^2 \qquad \text{(S4)}$$

where the subscript i refers to residue number, σ represents the standard error of the measurement, and α_1, α_2 are the scaling factors that define the relative contribution of LUV and SUV data to the total error function. Throughout this work, we report the values obtained with $\alpha_1 = \alpha_2 = 1$ ensuring the same weight for LUV and SUV data. $\Delta R_2^{\mathrm{calc}}$ in Eq. S4 is equal to $\Delta R_2^{\mathrm{overall}}$ of the main text and consists of two contributions,

$$\Delta R_2^{\mathrm{calc}} = \Delta R_2^{\mathrm{overall}} = \Delta R_2 + F^{\mathrm{iso}} \qquad \text{(S5)}$$

where ΔR_2 is calculated using Eq. S2.1 after propagation of Eq. S1 or Eq. S2.2, the relaxation rates R_2^{B} are calculated using Eq. S3 combined with Eq. 2 of the main text, and F^{iso} represents a uniform contribution to ^{15}N-ΔR_2 that takes into account the two additional binding modes of a given Ub_2 domain, i.e. modes (2) and (3) in Fig. 1D of the main text. Using Eqs. S5 and S2.2 and considering that in the macromolecular limit, only the spectral density at zero frequency contributes significantly to the relaxation rates, F^{iso} for SUV interactions, $F_{\mathrm{SUV}}^{\mathrm{iso}}$, can be recast, for example, in the following form,

$$F_{\mathrm{SUV}}^{\mathrm{iso}} \approx \Delta R_{2,\mathrm{SUV}}^{\mathrm{max}} - k_{\mathrm{on}}^{\mathrm{app,SUV}} K_{\mathrm{R}} (\tau_{\mathrm{C}}^{\mathrm{SUV}} + \tau_{\mathrm{w}}') / k_{\mathrm{off}} \qquad \text{(S6)}$$

where $\Delta R_{2,\mathrm{SUV}}^{\mathrm{max}}$ is chosen for simplicity because $[P_2(\cos\alpha)]^2 = 1$ in this case, K_{R} is a constant that incorporates dipolar and CSA relaxation constants in Eq. S3 and $S_{\mathrm{w}}^2 = 0.5$ ($K_{\mathrm{R}} \sim 0.775 \times 10^9$ s^{-1}), and the rest of the parameters are defined in the main text. A similar expression can be obtained for $F_{\mathrm{LUV}}^{\mathrm{iso}}$. Eq. S6 shows that F^{iso} is linearly anti-correlated with the apparent association rate constant $k_{\mathrm{on}}^{\mathrm{app}}$. Simultaneous determination of F^{iso} and $k_{\mathrm{on}}^{\mathrm{app}}$ by non-linear least squares fitting procedures is therefore very problematic without additional assumptions about either of the two parameters.

The set of global variable parameters of the fit thus comprises: $\left\{k_{on}^{app,SUV};k_{off};\tau_r;\theta;\varphi;F^{iso}\right\}$ when a single F^{iso} was used (i.e. when F_{LUV}^{iso} was assumed to be equal to F_{SUV}^{iso}), and $\left\{k_{off};\tau_r;\theta;\varphi;F_{LUV}^{iso};F_{SUV}^{iso}\right\}$ when this assumption was dropped, and the value of $k_{on}^{app,SUV}$ was fixed at the value obtained with $F_{LUV}^{iso}=F_{SUV}^{iso}$ minus four times the uncertainty in the fit (see main text). The minimizations of the target function in Eq. S4 were performed using home-written Matlab software (MathWorks Inc. MA). The uncertainties in the values of the optimized parameters, corresponding to confidence intervals of ±1 S.D., were determined from the variance-covariance matrix of the non-linear fit. Convergence of the solution was confirmed by varying initial values for all parameters and obtaining the same solution within the reported errors.

Relationship to spectral density function of Brainard & Szabo[S10]

In the notation adopted in this work (see Eq 2 of the main text), the correlation function, $C(t)$, derived by Brainard and Szabo[S10] to describe internal rotation of a bond vector around a symmetry axis defined in the molecular frame when the axis undergoes diffusive motions (wobbling) around its equilibrium position, has the following form,

$$C(t)=\exp(-t/\tau_C)\sum_{b=-2}^{2}\exp(-b^2t/6\tau_r)\left[d_{b0}^{(2)}(\alpha)\right]^2\left\{S_w^2+(1-S_w^2)\exp\left[-(t-b^2t/6)/\tau_w\right]\right\} \quad \text{(S7)}$$

where $d_{b0}^{(2)}(\alpha)$ are reduced elements of the Wigner rotation matrix of order 2:

$$d_{00}^{(2)}(\alpha)=(3\cos^2(\alpha)-1)/2;\ d_{\pm10}^{(2)}(\alpha)=\sqrt{3/2}\sin(\alpha)\cos(\alpha);\ d_{\pm20}^{(2)}(\alpha)=\sqrt{3/8}\sin^2(\alpha) \quad \text{(S8)}$$

After Fourier transformation of Eq. S7, we obtain,

$$\begin{aligned}J(\omega)=&S_w^2[P_2(\cos\alpha)]^2\frac{\tau_C}{1+(\omega\tau_C)^2}+S_w^2\left\{[3\cos^2\alpha\sin^2\alpha]\frac{\tau_r'}{1+(\omega\tau_r')^2}+[(3/4)\sin^4\alpha]\frac{\tau_r''}{1+(\omega\tau_r'')^2}\right\}\\&+(1-S_w^2)\left\{[P_2(\cos\alpha)]^2\frac{\tau_w'}{1+(\omega\tau_w')^2}+[3\cos^2\alpha\sin^2\alpha]\frac{\tau_w''}{1+(\omega\tau_w'')^2}+[(3/4)\sin^4\alpha]\frac{\tau_w'''}{1+(\omega\tau_w''')^2}\right\}\end{aligned} \quad \text{(S9)}$$

where

$\tau_r' = (1/\tau_C + 1/6\tau_r)^{-1}$; $\tau_r'' = (1/\tau_C + 2/3\tau_r)^{-1}$; $\tau_w' = (1/\tau_C + 1/\tau_w)^{-1}$;

$\tau_w'' = (1/\tau_C + 1/6\tau_r + 1/\tau_w - 1/6\tau_w)^{-1}$; $\tau_w''' = (1/\tau_C + 4/6\tau_r + 1/\tau_w - 4/6\tau_w)^{-1}$.

Note that the rotational and wobbling motions in Eq. S9 are inter-dependent, and *a-priori* no assumptions are necessary as to their relative time-scales (τ_r and τ_w). Eq S9 is to be compared with Eq 2 of the main text. As $\sum_{b=-2}^{2}\left[d_{b0}^{(2)}(\alpha)\right]^2=1$, if τ_r'' is assumed to be equal to τ_r' , then the second term in Eq S9 can be reduced to $S_w^2(1-[P_2(\cos\alpha)]^2)\frac{\tau_r'}{1+(\omega\tau_r')^2}$ which is equivalent to the second term in Eq 2 of the main text. The use of the spectral density function in Eq. S9 instead of that in Eq. 2 of the main text yields the parameters of exchange and dynamics of ubiquitin-liposome interactions that are very similar to those reported in the main text, except that the derived values of τ_r are approximately equal to 1/6 of the reported values by virtue of the different definitions of the effective correlation times of rotational motion in Eq S8 and Eq 2 of the main text.

Supplementary references:

(S1) Varadan, R.; Assfalg, M.; Haririnia, A.; Raasi, S.; Pickart, C.; Fushman, D. Solution Conformation of Lys63-linked Di-Ubiquitin Chain Provides Clues to Functional Diversity of Polyubiquitin Signaling. *J. Biol. Chem.* **2004**, *279*, 7055-7063.

(S2) Varadan, R.; Walker, O.; Pickart, C.; Fushman, D. Structural Properties of Polyubiquitin Chains in Solution. *J. Mol. Biol.* **2002**, *324*, 637-647.

(S3) Libich, D. S.; Fawzi, N. L.; Ying, J.; Clore, G. M. Probing the Transient Dark State of Substrate Binding to GroEL by Relaxation-Based Solution NMR. *Proc. Natl. Acad. Sci. U. S. A.* **2013**, *110*, 11361-11366.

(S4) Libich, D. S.; Tugarinov, V.; Clore, G. M. Intrinsic Unfoldase/Foldase Activity of the Chaperonin GroEL Directly Demonstrated Using Multinuclear Relaxation-Based NMR. *Proc. Natl. Acad. Sci. U. S. A.* **2015**, *112*, 8817-8823.

(S5) Fawzi, N. L.; Ying, J.; Torchia, D. A.; Clore, G. M. Kinetics of Amyloid β Monomer-to-Oligomer EXchange by NMR Relaxation. *J. Am. Chem. Soc.* **2010**, *132*, 9948-9951.

(S6) Delaglio, F.; Grzesiek, S.; Vuister, G. W.; Zhu, G.; Pfeifer, J.; Bax, A. NMRPipe: a Multidimensional Spectral Processing System Based on UNIX Pipes. *J. Biomol. NMR* **1995**, *6*, 277-293.

(S7) McConnell, H. M. Reaction Rates by Nuclear Magnetic Resonance. *J. Chem. Phys.* **1958**, *28*, 430-431.

(S8) Helgstrand, M.; Hard, T.; Allard, P. Simulations of NMR Pulse Sequences During Equilibrium and Non-Equilibrium Chemical Exchange. *J. Biomol. NMR* **2000**, *18*, 49-63.

(S9) Abragam, A. *Principles of Nuclear Magnetic Resonance*; Clarendon Press: Oxford, England, 1961.

(S10) Brainard, J. R.; Szabo, A. Theory for Nuclear Magnetic Relaxation of Probes in anisotropic Systems: Application of cholesterol in Phospholipid vesicles. *Biochemistry* **1981**, *20*, 4618-4628.

(S11) Cook, W. J.; Jeffrey, L. C.; Carson, M.; Chen, Z.; Pickart, C. M. Structure of a Di-Ubiquitin Conjugate and a Model for Interaction with Ubiquitin Conjugating Enzyme (E2). *J. Biol. Chem.* **1992**, *267*, 16467-16471.

(S12) Lai, M. Y.; Zhang, D.; Laronde-Leblanc, N.; Fushman, D. Structural and Biochemical Studies of the Open State of Lys48-Linked Di-Ubiquitin. *Biochim. Biophys. Acta* **2012**, *1823*, 2046-2056.

(S13) Weeks, S. D.; Grasty, K. C.; Hernandez-Cuebas, L.; Loll, P. J. Crystal Structures of Lys-63-Linked Tri- and Di-Ubiquitin Reveal a Highly Extended Chain Architecture. *Proteins* **2009**, *77*, 753-759.

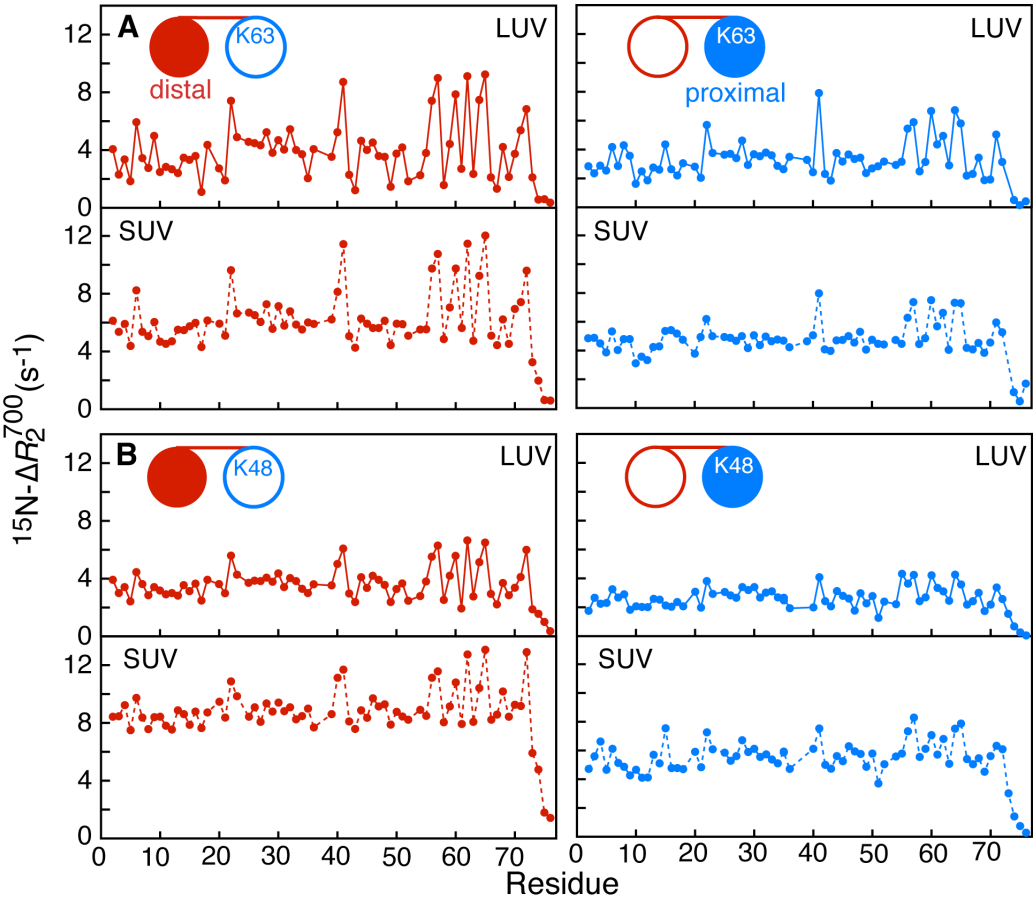

Figure S1. ^{15}N-ΔR_2 profiles obtained for the distal (shown in red) and proximal (in blue) domains of (**A**) K63-linked and (**B**) K48-linked di-ubiquitin (Ub_2) in the presence of negatively charged POPG LUVs (solid lines) and SUVs (dashed lines). The [^{15}N/ ^{2}H]-labeled domain in the various Ub_2 constructs is depicted by a filled-in circle in the cartoon representations shown in each panel. All the experimental data were collected at pH 6.8, 25 °C using 1:2 protein:lipid molar ratios at a protein concentration of 0.22 mM. The larger average value of ΔR_2 observed in the presence of SUVs compared to LUVs is the result of two competing factors: the population of the bound state, p_B and the total effective correlation time τ_C. Assuming the same k_{off} for LUVs and SUVs, the larger value of p_B for SUVs than LUVs is due to a larger value of k_{on}^{app}. k_{on}^{app} is the product of the second order association rate constant k_{on} and the concentration of nanoparticles. For a purely diffusion controlled reaction, the former is proportional to the radius of the nanoparticles, while the latter is inversely proportional to the cube of the radius of the nanoparticles. Thus, k_{on}^{app} is approximately proportional to the inverse square of the nanoparticle radius, which in this instance is ~16 times larger for SUVs than LUVs (see main text Table 1). τ_C, on the other hand, is dependent on both the rotational correlation time of the nanoparticle and the exchange rate (k_{ex} ~ k_{off}). From Table 1 of the main text the ratio of τ_C for LUVs to SUVs ranges from ~9 to ~13.

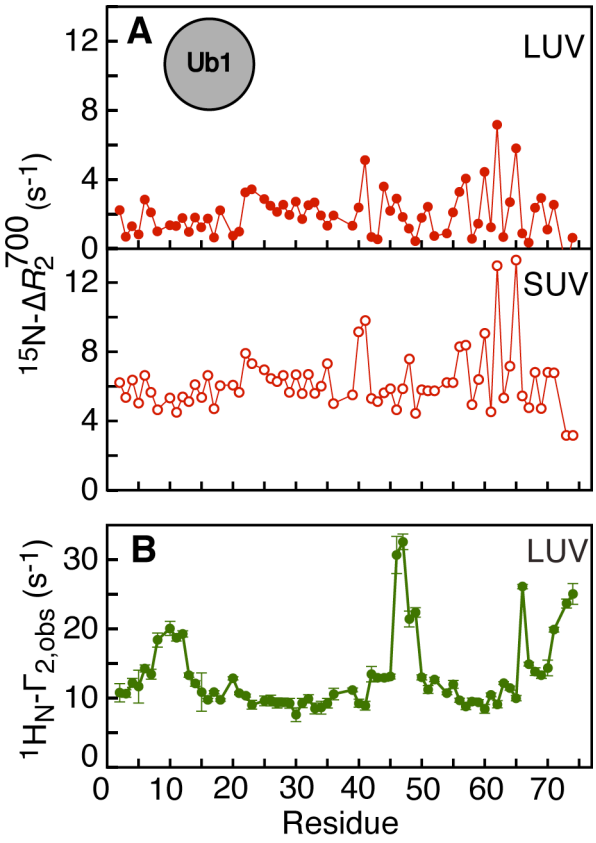

Figure S2. (**A**) ^{15}N-ΔR_2 profiles obtained for mono-ubiquitin (Ub_1) in the presence of POPG LUVs (filled symbols) and SUVs (open symbols). (**B**) Amide proton (^1H_N) intermolecular transverse PREs (Γ_2) observed for Ub_1 in the presence of negatively charged Gd^{3+}-tagged POPG LUVs. All the experimental data were collected at pH 6.8, 25 °C, and a 1:2 protein:lipid molar ratio with a protein concentration of 0.22 mM.

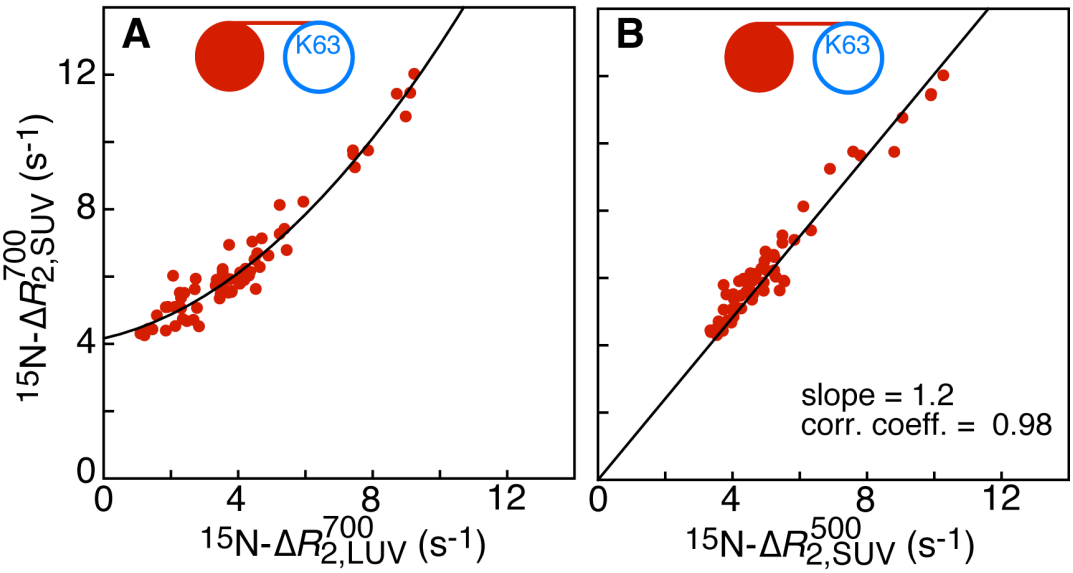

Figure S3. Dependence of ^{15}N-ΔR_2 on (**A**) nanoparticle size (SUV *vs.* LUV), and (**B**) magnetic field strength (700 and 500 MHz) measured on the [^{15}N/^{2}H]-labeled distal domain of K63-linked Ub_2 (represented by the filled-in circle in the cartoon representations shown in each panel). The average ratio of ^{15}N-ΔR_2 values at 700 to 500 MHz is 1.19, in good agreement with the calculated ratio of 1.20 from a relaxation mechanism based on the one-bond ^{1}H-^{15}N dipolar interaction and a -170 ppm ^{15}N chemical shift anisotropy. All the experimental data were collected at pH 6.8, 25 °C, and a 1:2 Ub_2:lipid molar ratio with a protein concentration of 0.22 mM.

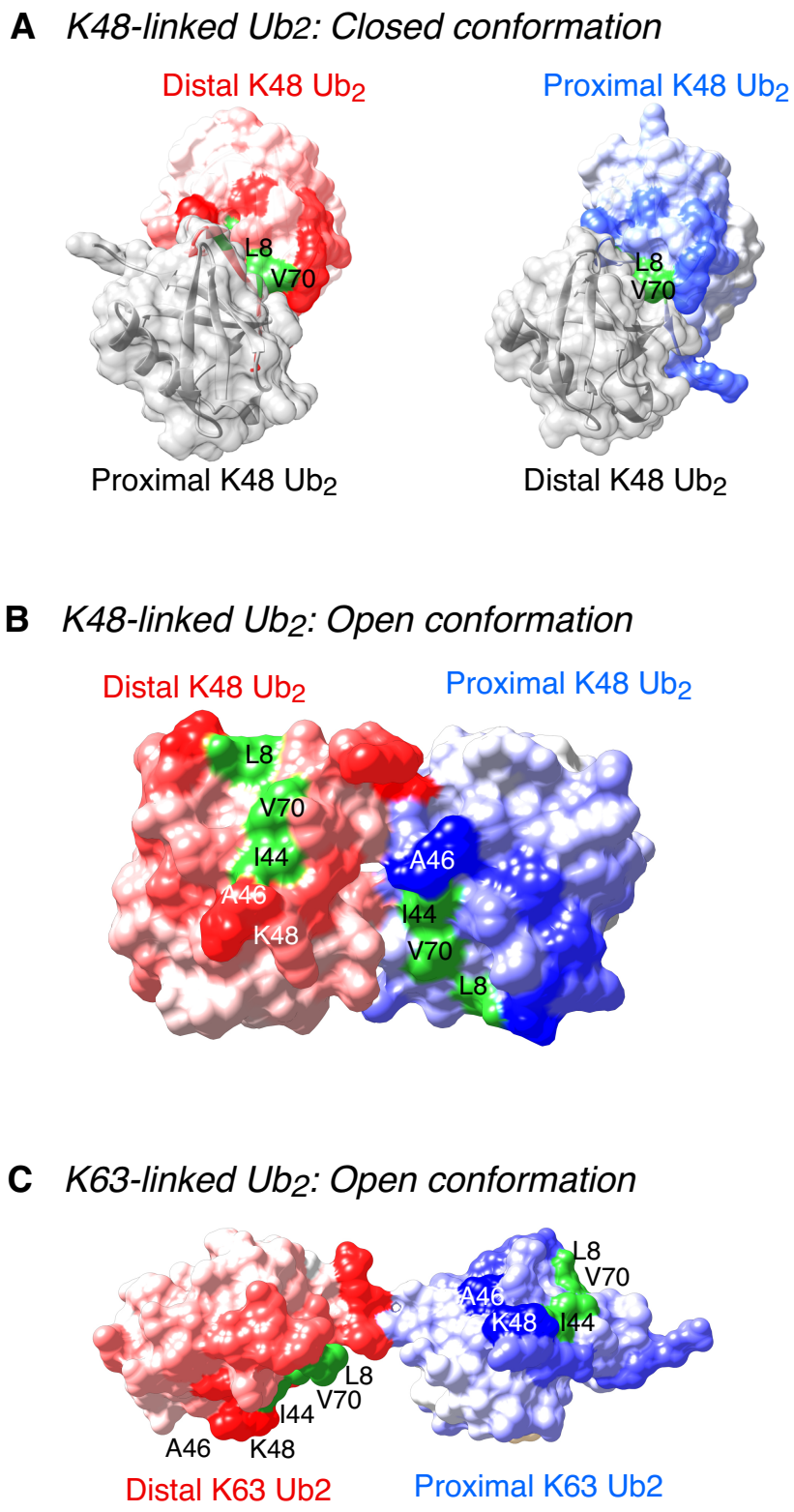

Figure S4. Mapping of $^{1}H_N$ intermolecular PREs on surface representations of K48- and K63-linked di-ubiquitin (Ub_2). Crystal structures of K48-linked Ub_2 in (**A**) the closed state (PDB ID 1AAR)[S11] and (**B**) the open state (PDB 3NS8).[S12] (**C**) Crystal structure of K63-linked Ub_2 (PDB ID 3H7P).[S13] PREs are color-coded from red (~18-20 s^{-1}) to white for the distal domains and from blue (~16-18 s^{-1}) to white for the proximal domains (the background is ~6.5 s^{-1} in both cases). Residues Leu^{8}, Ile^{44}, Val^{70} that form a surface hydrophobic patch in each Ub unit are shown in green.

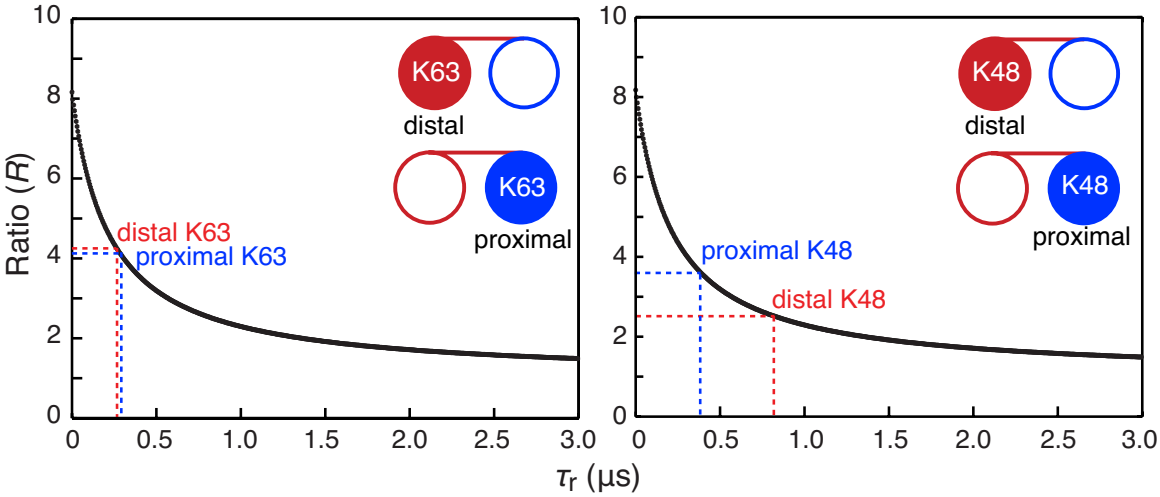

Figure S5. Calculated theoretical dependence of the ratio $R = (\Delta R_2^{\max} - F_{\text{SUV}}^{\text{iso}}) / (\Delta R_2^{\min} - F_{\text{SUV}}^{\text{iso}})$ on the correlation time of internal rotation τ_r for di-ubiquitin (Ub_2) on the surface of SUV nanoparticles. The ratios R are calculated with the exchange and dynamics parameters of interactions with SUV liposomes for K63- and K48-linked Ub_2 constructs (left and right panels, respectively) using the upper bounds for $F_{\text{SUV}}^{\text{iso}}$ reported in Table 1 of the main text. Experimental ratios R obtained in the presence of SUVs and the corresponding τ_r values (approximately equal to the lower bounds reported in Table 1 of the main text) are indicated for distal (red dashed lines) and proximal (blue dashed line) domains of the K63- and K48-linked Ub_2. The [^{15}N/^{2}H]-labeled domain is depicted by a filled-in circle (red, distal; blue, proximal) in the cartoon representation in each panel.